Together, these studies provided compelling evidence that HSPE is highly structure-dependent and can be effectively activated through phase or interface engineering. Shao and his co-workers demonstrated that metastable Hex-HfO_2 serves as an efficient spillover-active substrate when combined with Ru nanoclusters, enabling exceptional acidic HER performance. By contrast, Hwang and his co-workers used a Ni_3N/Ni_3Se_4 heterointerface to facilitate hydrogen spillover, overcoming kinetic limitations of selenide materials and achieving outstanding alkaline HER activity. These findings suggest that HSPE is a promising strategy for controlling multiple intermediate steps in HER and other hydrogenation reactions. Incorporating HSPE into catalyst design allows researchers to optimize rate-limiting steps, improve catalytic efficiency, and reduce precious metal loading. Ultimately, these advances may accelerate the development of high-performance, cost-effective hydrogen production technologies, contributing to the realization of a sustainable hydrogen economy. (Reported by Dessalew Dagnew Alemayehu and Chia-Hsin Wang)

This report features the work of Qi Shao and his collaborators, published in Adv. Mater. ***37****, 2415978 (2025); and the work of Bing Joe Hwang and his collaborators published in J. Am. Chem. Soc.* ***147****, 16047 (2025).*

TPS 44A Quick-scanning X-ray Absorption Spectroscopy
TLS 17C1 EXAFS
- XANES, EXAFS
- Materials Science, Catalysts

TLS 24A1 XPS, UPS, XAS, APXPS
- HR-XPS, NAP-XPS
- Materials Science, Surface Science, Catalysts

References

1. Q. Wang, J. Chen, S. Chen, D. Zhou, Y. Du, Y. Ji, Y. Xiong, J. Ke, W. Zhu, Y. Wang, D. Gao, W.-H. Huang, C.-W. Pao, Y. Sun, Y. Li, M. Shao, Z. Hu, X. Huang, Q. Shao, Adv. Mater. **37**, 2415978 (2025).
2. D. D. Alemayehu, M.-C. Tsai, M.-H. Tsai, C.-C. Yang, C.-C. Chang, C.-Y. Chang, E. A. Moges, K. Lakshmanan, Y. Nikodimos, W.-N. Su, C.-H. Wang, B. J. Hwang, J. Am. Chem. Soc. **147**, 16047 (2025).

Projection X-ray Microscopy: Illuminating Pathways to the Future of Energy Storage

Projection X-ray Microscopy opens a window into the hidden architecture of all-solid-state batteries, decoding how microstructure shapes performance.

To reduce air pollution, including CO, CH_4, NO_2, SO_2, Pb, and PM particles, the development and production of electric vehicles has risen in prominence, with high-capacity and safe batteries being the most important priorities. All-solid-state batteries (ASSBs) using intrinsically nonflammable solid-state electrolytes (SSEs) show promise as an alternative energy-dense storage solution due to their achievable higher energy density and improved safety. In contrast to conventional lithium-ion batteries, which benefit from facile ion transport *via* infiltration of liquid electrolytes into porous electrodes, ASSBs require physical contact between solid materials to facilitate the electrochemical reaction. Ideally, all components in ASSBs should exhibit fully densified microstructures that lack any porosity to maximize volumetric energy density. However, in practice, the mismatch in particle sizes and mechanical properties of materials induces unavoidable porosity or nonideal tortuosity within ASSBs. Either formed in the initial fabrication process or during battery operation due to volume changes of cathode/anode materials, the pores and gaps in the microstructure can lead to contact loss and propagation of fractures/cracks. Contact loss of active material reduces utilization, thus leading to lower reversible capacity and capacity loss. Meanwhile, voids and fracture formation within the microstructure could also lead to structural degradation or cell failure due to the disruption of ion percolation pathways. Thus, scaled-up tomography techniques will improve the understanding of ASSBs, elevating the technology's potential commercially. To quantitatively investigate the internal microstructure and its evolution within ASSBs during fabrication and cycling, three-dimensional (3D) micro-computed tomography and reconstruction techniques are essential.[1–3]

Ying Shirley Meng (University of Chicago, University of California San Diego, and Argonne National Laboratory, USA) and her team utilized **TPS 31A** projection X-ray microscopy (PXM) 3D tomography

at the NSRRC for structural analysis of ASSB at a pouch cell scale.[1] PXM tomography is a rapid (< 30 min), high resolution (1–26 μm) and large field of view (0.7–7 mm) technique for visualizing and quantifying key microstructural features, including overhang, porosity, contact loss, active surface area, and tortuosity in ASSB pouch cells. Moreover, PXM, as a nondestructive imaging technique allowing for *in situ* and *operando* characterization, can probe the internal microstructure of ASSBs without disassembling batteries. With the recent progression in ASSBs toward larger cell formats, analyzing the bulk microstructure of individual components is essential for gaining deeper insights into their electrochemical performance. In this work, they probed the microstructure of the ASSBs using the absorption contrast imaging mode of PXM. The demonstration of microstructure and quantitative analysis of the components within the argyrodite sulfide-based ASSB pouch cell, including μ-Si anode and $LiNi_{0.8}M_{0.1}Co_{0.1}O_2$ (NMC811) composite cathode, is shown in **Fig. 1**.

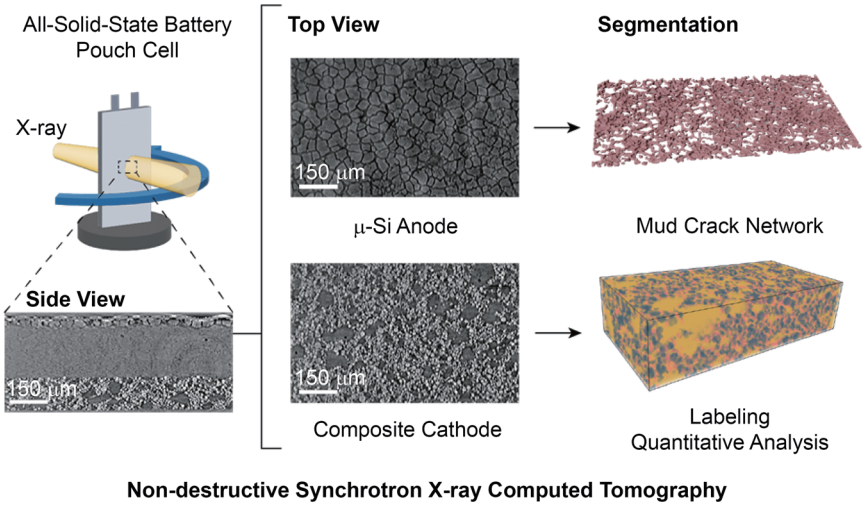

Fig. 1: PXM microstructure and quantitative analysis of the whole cell, μ-Si anode, and NMC811 composite cathode in ASSB pouch cell. [Reproduced from Ref. 1]

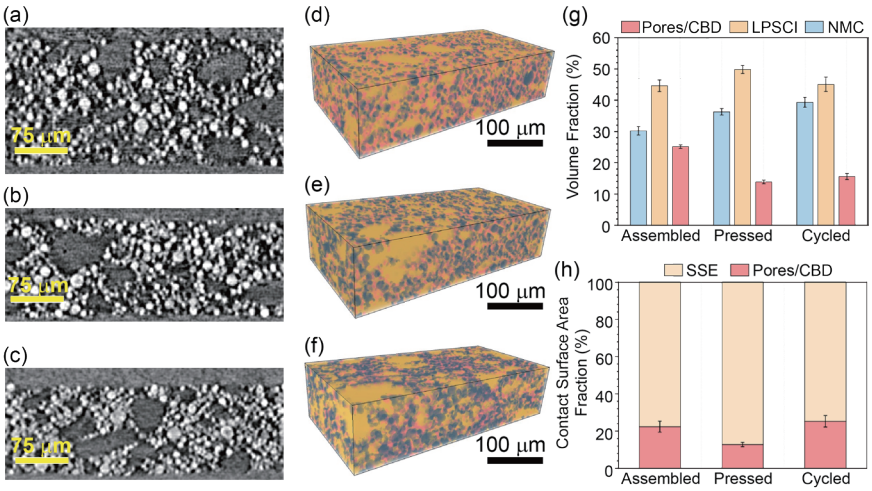

Fig. 2: Microstructure and quantitative analysis of composite cathode in pouch cells in different states: assembled, pressed, and cycled. The cross-section xy slice of (a) assembled, (b) pressed, and (c) cycled pouch cells showing the composite cathode. 3D segmented model of (d) assembled, (e) pressed, and (f) cycled pouch cells. In the 3D models, SSE is shown in yellow, NMC811 in blue, and pores/CBD in light red. (g) Volume fraction of each component within the composite cathode in different samples; (h) Contact surface area fraction of the active cathode material in the cathode composite electrode. [Reproduced from Ref. 1]

The quantitative analysis includes three stages: before cold isostatic pressing (CIP) at 500 MPa, referred to as "assembled"; after the CIP process, referred to as "pressed"; and post-C-rate test cycling at 5 MPa, referred to as "cycled". The microstructure of the three components, namely Si anode, SSE separator, and NMC811 composite cathode, during the three stages has been illustrated in detail. Specifically, the mud-crack network of the Si anode, porosity of the separator, and volume fraction and contact surface area fraction of the NMC811 composite cathode were characterized. The microstructure, volume fraction and contact surface area fraction of the NMC811 composite cathode are shown in **Fig. 2**. Cross-sectional (xy slice) PXM images provide a detailed view of the composite cathode microstructure (**Figs. 2(a)–2(c)**). Differences in X-ray absorption enable the precise identification of its components: the bright spherical particles correspond to NMC811, the gray regions represent the $LiPS_5Cl$ (LPSCl) separator, and the darkest areas represent the carbon binder domain (CBD), a mixture of pores, vapor-grown carbon fiber, and polytetrafluoroethylene (PTFE). The composite cathode electrode had an initial thickness of 180 μm within the assembled cell, which decreased to approximately 130 μm after the CIP process in both the pressed and cycled cells.

Figures 2(d)-2(f) for the segmentation results of the three stages show Pores/CBD, NMC811, and LPSCl as light red, blue, and yellow, respectively. The quantitative analysis of porosity for assembled, pressed, and cycled cells are 25.1, 13.8, and 15.6 vol%, respectively. The increased porosity of cycled compared to pressed cells could be attributed to the volume change

and potential particle cracks during charge/discharge processes of NMC811, creating gaps/voids in the microstructure that lead to the loss of physical contact, higher tortuosity, and charge transfer impedance, as well as lower active material utilization. Another important parameter governing the ASSBs' performance is the physical contact between the various composite components. **Figure 2(h)** compares the surface contact area of NMC811 particles within the composite cathode among the three samples. The fraction of the surface area of contact (between the NMC811 and SSE) of the assembled cells is 77.6%, which increased to 88.9% in pressed cells, and later decreased to 83.3% in cycled cells. The growth of the active surface area in pressed cells shows that the applied isostatic pressure compressed the pores and facilitated better physical contact between NMC811 and the SSE. This is imperative to maintain ionic transport and ensure better cathode active material utilization, namely higher reversible capacity. Meanwhile, the decline of the active surface area in cycled cells implies void formation, resulting from the volume change of NMC811 and plastic deformation of LPSCl.

To further explore the correlation between microstructure and electrochemical performance, significant efforts have been devoted to the computational modeling of ASSB degradation. The superiority of PXM tomography lies in its ability to access and analyze the microstructure and morphology of ASSBs with exceptional detail. PXM imaging and segmentation provide quantitative insights into critical microstructural information. Leveraging the nondestructive nature of tomography, the 3D PXM models at different states of charge or cycles can be integrated with computational modeling to understand the chemo-mechanical degradation mechanism of ASSBs. PXM-segmented 3D models provide true-to-life geometry and authentic microstructure representation, offering a practical starting point for advancing simulation and modeling. **Figure 3** outlines a proposed multiphysics simulation workflow that incorporates PXM reconstructed 3D microstructures to study ASSB degradation mechanisms. The approach starts with reconstructing the measured PXM slices to obtain realistic 3D models of ASSB microstructures. Subsequently, the surface representation of each segmented particle and features can be easily converted using commercially available software.

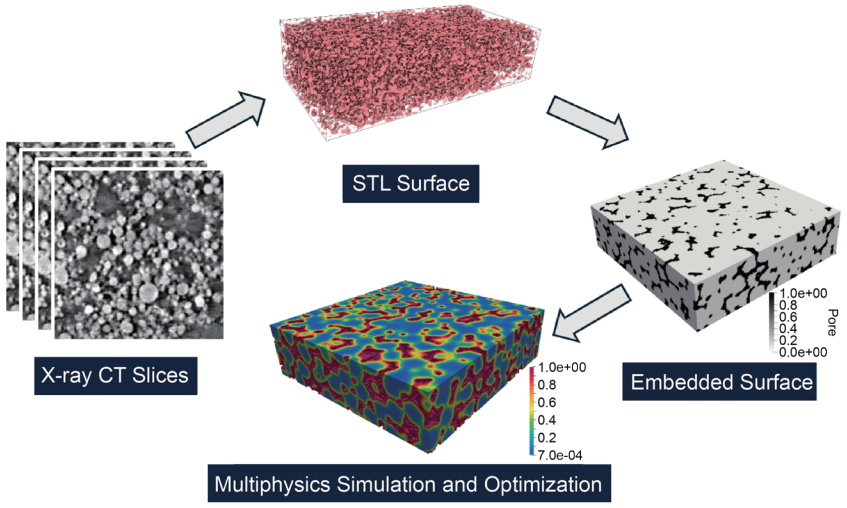

Fig. 3: Multiphysics simulation workflow using realistic PXM reconstructed 3D models. Schematic showing workflow of using real 3D PXM models for multiphysics simulation in four steps: obtaining PXM slices, generating surface mesh file, regularizing noisy surface representations, and multiphysics simulation and optimization for ASSB degradation mechanism study. The colormaps in the simulation model represent different phases including particles, the void, and the regularized transition zone. [Reproduced from Ref. 1]

In summary, PXM offers quantitative insights into the ASSB microstructure, including (1) porosity of individual components, (2) particle size distribution for tortuosity analysis, (3) volume fraction in the composite cathode, (4) contact surface area between active cathode materials and voids or solid state electrolytes, and (5) delamination at the Cu current collector and the Si anode interface. PXM investigation on ASSBs at the pouch cell level provides industry-relevant insights, leading the design and engineering of robust and high performance ASSBs for practical applications. (Reported by Yen-Fang Song)

This report features the work of Ying Shirley Meng and his collaborators published in ACS Energ. Lett. ***10****, 3459 (2025).*

TPS 31A Projection X-ray Microscopy

- PXM
- Chemistry Engineering, Materials Science, Green Sustainable Chemical Process

References

1. C.-J. Huang, J. A. S. Oh, M. Vicencio, T. Hu, H. Yang, J. N. Burrow, Y.-F. Song, G.-C. Yin, P. Shevchenko, K. M. Wiaderek, B.-J. Hwang, Y. S. Meng, ACS Energ. Lett. **10**, 3459 (2025).
2. H. Chen, H.-W Liu, Y.-C. Lu, P.-J. Yu, C.-H Liao, C.-C. Wang, T.-S. Chan, H.-S. Sheu, P.-Y. Chang, J.-L. Chen, S.-C. Haw, G.-C. Yin, Y.-F. Song, C.-W. Pao, N.-L. Wu, Chem. Eng. J. **519**, 165314 (2025).
3. H.-W Liu, H. Chen, S. Thi, P.-J. Yu, J.-L. Chen, C.-W. Pao, P.-Y. Chang, S.-C. Haw, Y.-F. Liao, Y.-C. Shao, G.-C Yin, Y.-F. Song, S.-K. Parthasarathi, Y.-T. Weng, N.-L. Wu, Compos. Pt. B **293**, 112133 (2025).